J. Fluid Mech. (1969), *vol.* 37, *part* 2, *pp.* 383–413
Printed in Great Britain

Rough wall turbulent boundary layers

By A. E. PERRY, W. H. SCHOFIELD AND P. N. JOUBERT
Department of Mechanical Engineering, University of Melbourne

(Received 16 August 1968)

This paper describes a detailed experimental study of turbulent boundary-layer development over rough walls in both zero and adverse pressure gradients. In contrast to previous work on this problem the skin friction was determined by pressure tapping the roughness elements and measuring their form drag.

Two wall roughness geometries were chosen each giving a different law of behaviour; they were selected on the basis of their reported behaviour in pipe flow experiments. One type gives a Clauser type roughness function which depends on a Reynolds number based on the shear velocity and on a length associated with the size of the roughness. The other type of roughness (typified by a smooth wall containing a pattern of narrow cavities) has been tested in pipes and it is shown here that these pipe results indicate that the corresponding roughness function does not depend on roughness scale but depends instead on the pipe diameter. In boundary-layer flow the first type of roughness gives a roughness function identical to pipe flow as given by Clauser and verified by Hama and Perry & Joubert. The emphasis of this work is on the second type of roughness in boundary-layer flow. No external length scale associated with the boundary layer that is analogous to pipe diameter has been found, except perhaps for the zero pressure gradient case. However, it has been found that results for both types of roughness correlate with a Reynolds number based on the wall shear velocity and on the distance below the crests of the elements from where the logarithmic distribution of velocity is measured. One important implication of this is that a zero pressure gradient boundary layer with a cavity type rough wall conforms to Rotta's condition of precise self preserving flow. Some other implications of this are also discussed.

1. Introduction

Two types of roughness

The framework of rough-wall flow analysis was established by Nikuradse (1933) who investigated flow in sand-roughened pipes. He found that with increasing Reynolds number the flow behaviour deviated from the turbulent smooth-wall law and depended on the relative scale of the roughness k/d (k is roughness scale and d pipe diameter) as well as the Reynolds number. At higher Reynolds number the flow becomes independent of viscosity and is a function of k/d alone as shown in figure 1. Flow dependent on k/d alone was termed 'fully rough' while flow dependent on both k/d and Reynolds number was termed transition flow.

Another important result of Nikuradse was that the smooth-wall velocity defect law applied to the bulk of the flow irrespective of the scale (k) of the roughness. The effect of roughness on the velocity profile shape was thus, like viscosity (ν), confined to a thin wall layer. Perry & Joubert (1963) therefore proposed to account for the effect of roughness on the bulk of the flow by simply using a

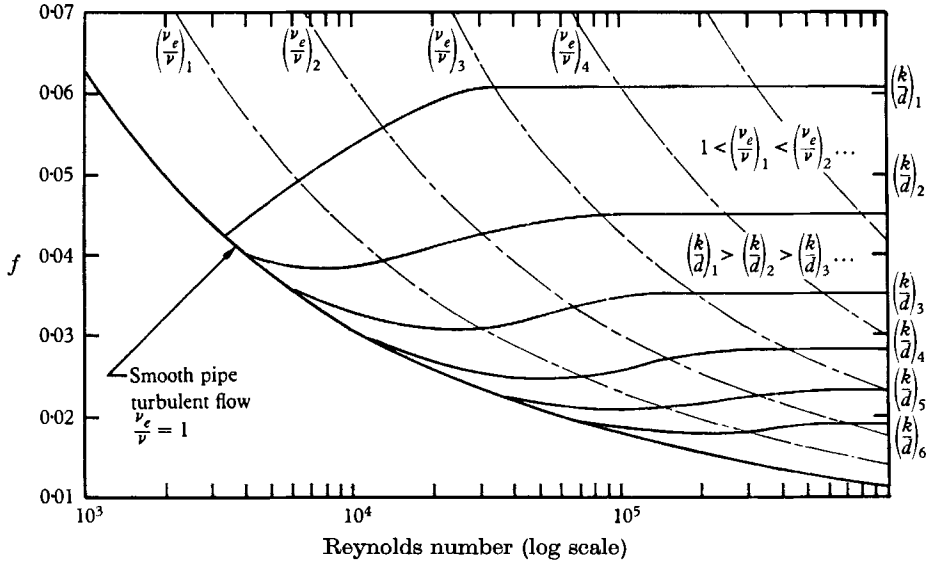

FIGURE 1. Nikuradse's (1933) pipe results. 'k' type roughness.

modified fluid viscosity ν_e. The form of the logarithmic velocity distribution for flow over rough walls given by Clauser (1954),

$$\frac{u}{u_\tau} = \frac{1}{\kappa}\log_e\left(\frac{yu_\tau}{\nu}\right) + A - \frac{\Delta u}{u_\tau}\left[\frac{ku_\tau}{\nu}\right], \dagger \tag{1}$$

(where $u_\tau = \sqrt{(\tau_0/\rho)}$, τ_0 being the wall shear stress and ρ the fluid density, $(\Delta u/u_\tau)\,[ku_\tau/\nu]$ the roughness function which is zero for smooth walls and κ, A are universal constants) can then be written simply as

$$\left.\begin{aligned} \frac{u}{u_\tau} &= \frac{1}{\kappa}\log_e\left(\frac{yu_\tau}{\nu_e}\right) + A, \\ \text{where} \quad \frac{\nu}{\nu_e} &= \exp\left(\kappa\frac{\Delta u}{u_\tau}\left[\frac{ku_\tau}{\nu}\right]\right) \end{aligned}\right\} \tag{2}$$

and it follows that $\nu_e/\nu = 1$ for smooth walls. Hama (1954) showed from the results of an extensive experimental programme that (1) and the Clauser form of the roughness function for fully rough flow,

$$\frac{\Delta u}{u_\tau} = \frac{1}{\kappa}\log_e\left(\frac{ku_\tau}{\nu}\right) + \text{constant}, \tag{3}$$

are both universal for a given roughness geometry in pipe, channel and zero pressure gradient boundary-layer flow. Perry & Joubert (1963) showed that the

† Throughout this paper square brackets will denote a functional dependence.

universality extends to boundary-layer flow in adverse pressure gradients. It should therefore be possible to determine the roughness function for boundary-layer flow from a simple pipe test. A convenient method of doing this is illustrated in figure 1 where Nikuradse's pipe results are shown on axes friction factor (f) *versus* log Reynolds number (R). In this paper f is defined by $\sqrt{(8/f)} = U_b/u_\tau$, where U_b is the bulk mean velocity given by

$$U_b = \frac{1}{A}\int_A (u)\,dA$$

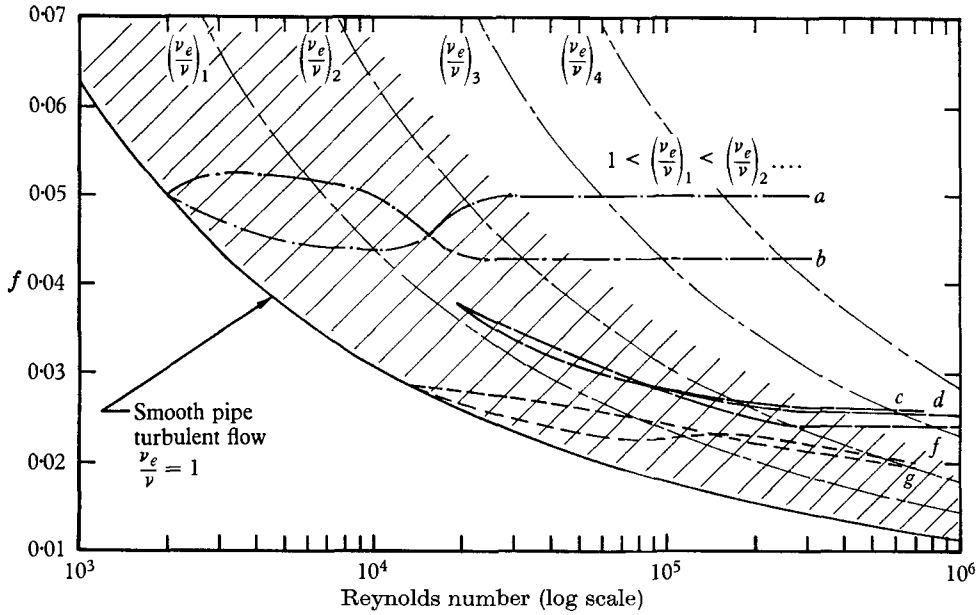

FIGURE 2. Flow in pipes with depression or groove type roughness ('d' type roughness). Values of relative roughness (k/d) for results shown: a, 0·0125; b, 0·0185; c, 0·0204; d, 0·0112; e, 0·0056; f, 0·0162; g, 0·0337. —·—, Sams (1952); ——, Streeter & Chu (1949); – – – –, Ambrose (1954).

and A is the flow area; the Reynolds number here is $U_b d/\nu$. Also shown on figure 1 are curves for turbulent 'smooth wall' flow for various modified fluid viscosities ($\nu_e/\nu \neq 1$). From (2) the rough-wall velocity profiles can be collapsed onto the smooth-wall results by replacing ν by ν_e. It follows therefore that a rough-wall friction factor *versus* Reynolds number curve for constant ν_e is identical to the smooth-wall curve with ν replaced by ν_e in the Reynolds number. Hence the curves of constant ν_e/ν on figure 1 are simply the smooth-wall friction factor graph shifted bodily sideways by $\log \nu_e/\nu$. Equation (2) shows that these curves are also contours of $\Delta u/u_\tau$. By plotting experimental data on this chart it is therefore possible to read off the appropriate value of $\Delta u/u_\tau$ and to calculate the product $(R)(\sqrt{f})(k/d)$ which is proportional to ku_τ/ν. The resulting graph of $\Delta u/u_\tau$ *versus* ku_τ/ν will be universal for a given roughness geometry and will give the relationship for both the transition and fully rough régimes in terms of variables required for boundary-layer analysis.

The above method of pipe to boundary-layer correlation is valid provided the roughness behaviour follows the usual Clauser or Nikuradse scheme. However, Streeter & Chu (1949) and Ambrose (1956) have reported examples of roughness whose friction factor–Reynolds number characteristics are insensitive to the relative scale k/d. This type of roughness is characterized by a smooth surface with a series of depressions or grooves within which the outer flow generates stable vortices. Their results are shown in figure 2. In this case as will be shown later, ν_e/ν and hence $\Delta u/u_\tau$ is a function of the product $R\sqrt{f}$ alone which is proportional to du_τ/ν. The resulting roughness function graph (for a given geometry) is a single curve as before, but with an abscissa of du_τ/ν instead of ku_τ/ν. As the length scale (d) used to describe the roughness function is associated with the outer flow this result appears to be inconsistent with Prandtl's 'law of the wall' developed by Nikuradse (1933) and Clauser (1954) for rough walls. Also for application to boundary-layer flow the curve obtained for the roughness function is of little use as pipe diameter has no obvious equivalent in boundary layers. For the special case of an equilibrium boundary layer the results may possibly correlate with δ, the boundary-layer thickness, but such a correlation seems most unlikely for the arbitrary pressure gradient case. In this paper these two types of roughness action will be termed 'k' type and 'd' type, the symbols denoting the significant length scale involved.

Measurement of wall shear stress on rough walls

A major experimental difficulty in studying rough-wall boundary layers in non-zero pressure gradients is to measure the local wall shear stress accurately. Smooth-wall techniques such as Preston or Stanton tubes require a knowledge of the roughness function to give an answer. Momentum integral methods, though useful for zero pressure gradient boundary layers, become highly inaccurate when applied to boundary-layer development in pressure gradients. Another possibility is the graphical method introduced by Clauser (1954) for finding wall shear stress of smooth-wall boundary layers. The Clauser method determines the local skin-friction coefficient by plotting the mean velocity profile on axes u/U_1 *versus* $\log_{10}(yU_1/\nu)$, where U_1 is the local free-stream velocity. The logarithmic distribution of velocity near the wall appears as a straight line on these axes and it is the position and slope of this line that determines the local skin-friction coefficient. However, boundary layers on rough walls introduce two additional variables to the plot.

First, there is the roughness function $\Delta u/u_\tau$ which shifts the logarithmic portion of the mean velocity profile on the plot away from the position of the corresponding smooth-wall profile, as given by (1). As the determination of $\Delta u/u_\tau$ is one of the aims of roughness research, the amount the profile is shifted on the Clauser plot is unknown.

Secondly, Moore (1951) showed that a boundary layer on a rough wall behaves as if its origin is located some distance (ϵ) below the crests of the elements. The distance ϵ, which will be referred to as the error in origin, defines an origin for the profiles that will give the logarithmic distribution of velocity near the wall. The

error in origin can be considered as a measure of the interaction between the mean flow and the roughness. As such it seems that ϵ should be related to the roughness function. To the authors' knowledge no such relation has been published.

Due to these two additional variables ($\Delta u/u_\tau, \epsilon$) Clauser's method for finding the wall shear stress becomes imprecise as it is found that a large range of possible combinations of the wall parameters ($\tau_0, \Delta u/u_\tau, \epsilon$) will give nearly straight lines on the Clauser plot and any of them could be interpreted as the correct logarithmic distribution. Perry & Joubert studied the case of rough-wall boundary layers in adverse pressure gradients, finding the wall parameters by an extension of the Clauser plot which employed the properties of the wake function (Coles 1956). The method was not entirely satisfactory as the wake function is not truly universal at the outer edge of the boundary layer. As a means of finding the wall shear stress on a rough-wall boundary layer the Clauser method is therefore of limited use. However, if the wall shear stress is known by some other method the Clauser plot affords a fairly accurate means of determining the two other wall variables ϵ and $\Delta u/u_\tau$. This approach was used in the present work.

Aims

The aims of this work are: (i) to determine whether the roughness function $\Delta u/u_\tau$, for a zero pressure gradient boundary-layer flow on a '*d*' type rough wall is a function of ($\delta u_\tau/\nu$) alone; (ii) to determine a correlating length scale for $\Delta u/u_\tau$ in an arbitrary pressure gradient boundary-layer flow on a '*d*' type rough wall; (iii) to determine the relationship of $\Delta u/u_\tau$ to the error in origin of the logarithmic velocity profiles (ϵ); (iv) to develop a method of measuring local wall shear stress on rough walls which avoids the use of the momentum integral equation and assumptions concerned with velocity profile similarity laws.

2. '*d*' type roughness

Previous work

Published evidence of '*d*' type roughness behaviour is limited to pipe flow.

Sams (1952) considered flow in two pipes that had been roughened by cutting square threads on their internal surfaces. The two thread forms were approximately similar differing in scale by 50 %. However, the published photographs show that the form of the threads was not accurately controlled and this is reflected in the results which show considerable scatter. The mean curves fitted to the results (see figure 2) do show a distinct trend that is opposite to that of the Nikuradse curves; the results for the larger relative roughness scale (k/d) having the lower friction factors (f).

Streeter & Chu (1949) also investigated flow in three pipes with square-threaded internal roughness. The accuracy of the thread form cannot be assessed from the report but the results show little scatter. In this case a variation by a factor of nearly 4 in the relative roughness scale resulted in a friction factor change of approximately 5 %. An equivalent change of relative roughness in Nikuradse's sand grain geometry would give a friction factor change of approximately 25 %. The trend of the results did, however, agree with that of Nikuradse's

results. In this work cursory velocity profiles (involving only thirteen measuring points per profile) were taken.

Ambrose (1956) reported a detailed investigation of flow in pipes fitted with liners in which a regular pattern of circular holes had been drilled. The friction factor was determined by the pressure-drop method and detailed velocity traverses were taken. Unfortunately only two pipe liners having the same roughness pattern but different relative scales were tested. The results (figure 2) show that initial transition from smooth-wall flow was dependent on the scale of the roughness. At higher Reynolds numbers the results for the two scales of roughness are identical, but as they do not fall on a horizontal straight line they are not viscosity independent. Ambrose (1954) considered that this higher Reynolds number behaviour indicated a type of roughness action that did not become viscosity independent. However, as his results all lie within the limits for transitional flow suggested by Colebrook & White (1937), shown as the shaded region in figure 2, it is possible that viscosity independent flow is delayed until very high Reynolds numbers for this particular roughness geometry.

Implication of results

The results of Ambrose and Streeter & Chu can be used to show the functional dependence of the roughness on the pipe diameter which was indicated in the introduction.

Near the wall of the pipe these results show that the mean velocity profiles follow the logarithmic distribution and the outer flow follows the usual velocity defect law. Hence, the whole flow beyond a thin sublayer can be expressed as

$$\frac{u}{u_\tau} = \frac{1}{\kappa}\log_e\left(\frac{yu_\tau}{\nu}\right) + A - \frac{\Delta u}{u_\tau} + h\left[\frac{2y}{d}\right], \tag{4}$$

where h is a deviation function introduced by Millikan (1938) to describe that part of the velocity profile which departs from the logarithmic law in the core region of the pipe. The function $h[2y/d]$ is zero if $2y/d < \xi$, where ξ is of the order of 0·2. At $y = \frac{1}{2}d$; $(u = U_1)$ (4) becomes

$$\frac{U_1}{u_\tau} = \frac{1}{\kappa}\log_e\left(\frac{du_\tau}{2\nu}\right) + A - \frac{\Delta u}{u_\tau} + h(1). \tag{5}$$

By subtracting (4) from (5) the velocity defect form is obtained

$$\frac{U_1 - u}{u_\tau} = -\frac{1}{\kappa}\log_e\left(\frac{2y}{d}\right) + h(1) - h\left(\frac{2y}{d}\right)$$

and integration of this equation over the flow area (see Perry 1964), gives

$$\frac{U_1 - U_b}{u_\tau} = \frac{3}{2\kappa} + h(1) + \eta, \tag{6}$$

where η is a constant. Substitution of (5) into (6) gives an expression for the roughness function:

$$\frac{\Delta u}{u_\tau} = \frac{1}{\kappa}\log_e\left(\frac{du_\tau}{2\nu}\right) + A - \frac{3}{2\kappa} - \eta - \frac{U_b}{u_\tau}. \tag{7}$$

If the friction factor (f) and hence U_b/u_τ is not a function of k/d and depends on Reynolds number ($U_b d/\nu$) alone, then U_b/u_τ will be a unique function of du_τ/ν. Equation (7) can then be written as

$$\frac{\Delta u}{u_\tau} = \frac{1}{\kappa}\log_e\left(\frac{du_\tau}{2\nu}\right) + A - \frac{3}{2\kappa} - \eta - \frac{U_b}{u_\tau}\left[\frac{du_\tau}{\nu}\right].$$

A substitution of the smooth wall condition ($\Delta u/u_\tau = 0$) into (7) gives

$$\frac{U_b}{u_\tau} = \sqrt{\left(\frac{8}{f}\right)} = \frac{1}{\kappa}\log_e\left(\frac{du_\tau}{2\nu}\right) + A - \frac{3}{2\kappa} - \eta,$$

which has previously been derived by one of us (Perry 1964). At sufficiently high Reynolds numbers, U_b/u_τ is constant and (5) then becomes

$$\frac{\Delta u}{u_\tau} = \frac{1}{\kappa}\log_e\left(\frac{du_\tau}{\nu}\right) + G, \tag{8}$$

where G is a constant for a given roughness and duct geometry.† Equation (8) has the same form as (3) but k is replaced by d.

The two facts, first, that the external length scale d appears in the equation for the roughness function and second, that the velocity distribution near the wall is logarithmic, lead to a partial understanding of how the parameter 'd' affects the flow. The mean flow near the wall may be expressed as

$$\frac{u}{u_\tau} = \phi_1\left[\frac{yu_\tau}{\nu}, \frac{du_\tau}{\nu}\right]. \tag{9}$$

To obtain the observed logarithmic distribution by a dimensional argument, it is necessary to assume that in a region above the roughness, mean relative motions are independent of length scales associated with the behaviour of flow at the boundary. Furthermore, 'd' must be classed with ν/u_τ as a boundary-length scale and hence

$$\frac{\partial u}{\partial y} = \phi_2[y, u_\tau \text{ alone}]$$

and by dimensional analysis

$$\frac{\partial u}{\partial y} = \frac{1}{\kappa y}. \tag{10}$$

Integration of (10) gives

$$\frac{u}{u_\tau} = \frac{1}{\kappa}\log_e(y) + \text{constant} \tag{11}$$

A comparison of (9) and (11) leads to

$$\frac{u}{u_\tau} = \frac{1}{\kappa}\log_e\left(\frac{yu_\tau}{\nu}\right) + A - \frac{\Delta u}{u_\tau}\left[\frac{du_\tau}{\nu}\right]. \tag{12}$$

Beyond the region of the law of the wall, d will have an influence not only on the boundary condition for (11) but will also control the mean relative motions. The

† This analysis is for a circular pipe but could probably be extended to non-circular ducts. To do this the variation of wall shear stress around the periphery of a non-circular duct would have to be taken into account (see Perry 1964).

velocity distribution must then include Millikan's deviation function $h[2y/d]$ as given in (4). The influence of 'd' at the boundary of the flow is examined further in the next section.

3. Proposed structure of 'k' and 'd' type rough-wall flow

Pipe flow

Only fully rough flow is considered with figures 3 and 4 defining the variables used. For simplicity the following work is restricted to two-dimensional strip roughness.

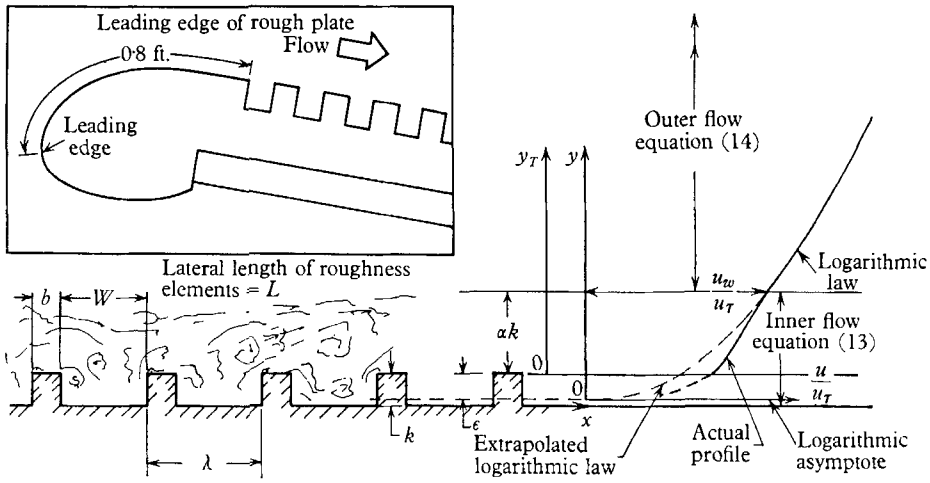

FIGURE 3. 'k' type roughness.

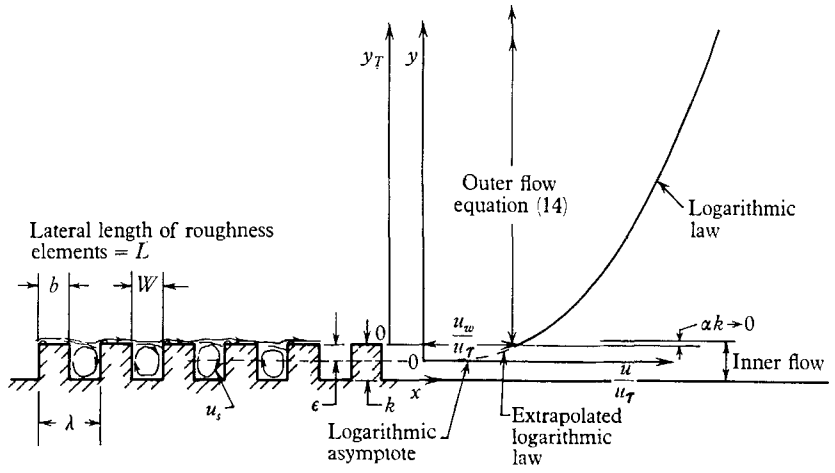

FIGURE 4. 'd' type roughness.

In the case of 'k' type roughness (figure 3), eddies with a length scale proportional to 'k' are assumed to be shed into the flow above the crests of the elements. Further away from the crests, this roughness sublayer structure blends smoothly into the flow which is described by the velocity defect law. It is then assumed that

this inner flow has a characteristic velocity scale u_τ and a single length scale k and hence

$$\frac{u}{u_\tau} = f\left[\frac{y_\tau}{k}\right]. \tag{13}$$

The outer flow is described by (4) which for $2y/d < \xi$ can be written as

$$\frac{u}{u_\tau} = \frac{1}{\kappa}\log_e\left(\frac{(y_T+\epsilon)u_\tau}{\nu}\right) + A - \frac{\Delta u}{u_\tau}, \tag{14}$$

but will be valid only if the two regions blend along a line that has no periodic disturbances of wavelength λ. That is, (14) is valid only if the constant α is 'sufficiently large'. At $y_T = \alpha k$, $u/u_\tau = u_w/u_\tau = \beta$ by (13), where β is constant. The parameter u_w/u_τ will be referred to as the 'surface drag coefficient' and is analogous to the non-dimensional velocity at the outer edge of the viscous sublayer for flow over a smooth surface. In the smooth wall case $y = \alpha\nu/u_\tau$ at the outer edge of the viscous sublayer and hence ν/u_τ is analogous to k for 'k' type rough wall flow.

Equating the velocities given by the inner and outer flow (at $y_T = \alpha k$) leads to

$$\frac{\Delta u}{u_\tau} = \frac{1}{\kappa}\log_e\left\{\left(\frac{\alpha k+\epsilon}{\nu}\right)u_\tau\right\} + F, \tag{15}$$

where F is constant. A comparison of velocity gradients given by (13) and (14) shows that ϵ is proportional to k which puts (15) into the form of (3). Alternatively (15) could be written as

$$\frac{\Delta u}{u_\tau} = \frac{1}{\kappa}\log_e\left(\frac{\epsilon u_\tau}{\nu}\right) + C_k, \tag{16}$$

where C_k is a constant, characteristic of the roughness.

On a 'd' type rough wall the elements are more closely spaced and stable vortices are set up in the grooves and eddy shedding from the elements into the flow will be negligible. The outer flow rides relatively undisturbed over the crests of the elements and the distance αk in figure 3 and equation (15), approaches zero. It has been found experimentally (see §5) that for the case of 'd' type rough walls, the drag on the roughness elements is extremely sensitive to vertical misalignment of the element crests.† It is plausible that an effect similar to that produced by vertical misalignment occurs if the instantaneous direction of the streamlines above the grooves are changed by the large-scale vertical components of velocity impressed from the outer flow. In this case a length scale associated with these outer flow motions will govern the flow at the boundary.

If a 'd' type rough surface has a constant 'surface drag coefficient' u_w/u_τ (as in smooth and 'k' type rough wall flow), it follows directly from (15) that for αk negligibly small

$$\frac{\Delta u}{u_\tau} = \frac{1}{\kappa}\log_e\left(\frac{\epsilon u_\tau}{\nu}\right) + C_d, \tag{17}$$

where C_d is a constant, characteristic of the roughness. The procedure followed in the 'k' type analysis could not be followed in this case because even if (13) was

† In this and subsequent contexts 'vertical' means 'in a direction normal to the surface of the main plate'.

valid within the grooves (i.e. for negative y_T), as d governs the flow near the crests the velocity gradients given by (13) and (14) cannot be equated. In the 'k' analysis equating velocity gradients gave the result that ϵ was proportional to k. The apparent independence of ϵ with k for 'd' type rough wall flow implies that characteristic velocity gradients within the grooves (given by $u_s/k \simeq u_w/k$) are not related to gradients of velocity given by the outer flow relations above the crests. Results in §5 show that C_d (and hence u_w/u_τ) is universal for a given roughness geometry even for boundary layers developing in strong arbitrary adverse pressure gradients.

For a general flow situation ϵ cannot be predicted at the present state of knowledge. However, for the particular case of pipe flow it appears that ϵ is proportional to the pipe diameter, d (from a comparison of (8) and (17)). This proportionality is consistent with the idea that the large-scale motions from the outer flow have an influence at the surface since, by Townsend's (1956) Reynolds number similarity hypothesis, these large-scale motions have characteristic velocity and length scales of u_τ and d. They could probably be described as the inactive components of the flow (Townsend 1961) since they appear to penetrate through the logarithmic region without affecting it except by their influence on the roughness function.

Boundary-layer flow on a 'd' type rough wall

In the case of boundary-layer flow no obvious equivalent to 'd' exists and there are many external measurable length scales that could influence ϵ. This is especially true in the case of boundary layers developing in arbitrary pressure gradients. However, for the particular case of equilibrium boundary layers all large-scale motions should scale approximately to one local length scale and one local velocity scale. One important case of equilibrium layers is the zero pressure gradient layer and here it is well established that mean relative motions scale according to a boundary-layer thickness (δ or Clauser's (1954) thickness Δ_c defined on an integral basis) and the local wall shear velocity u_τ, as given by the velocity defect law (Hama 1954). There is also evidence, although it is not conclusive, that the distributions of the r.m.s. values of the fluctuating velocity components if scaled with δ and u_τ are universal for both smooth and rough walls. This was a conclusion of Hinze (1959) after comparing the rough wall data of Corrison & Kistler (1954) with the smooth wall data of Klebanoff (1955). If this type of similarity exists for mean and fluctuating components in the case considered here then ϵ should be proportional to δ. Equation (17) would then be written as

$$\frac{\Delta u}{u_\tau} = \frac{1}{\kappa}\log_e\left(\frac{\delta u_\tau}{\nu}\right) + D, \tag{18}$$

where D is a constant, characteristic of the roughness geometry and of zero pressure gradient boundary layers. This assumption has interesting consequences. (i) The equivalent expression of (4) for a boundary layer is

$$\frac{u}{u_\tau} = \frac{1}{\kappa}\log_e\left(\frac{yu_\tau}{\nu}\right) + A - \frac{\Delta u}{u_\tau} + g\left[\frac{y}{\delta}\right], \tag{19}$$

where $g[y/\delta]$ is the corresponding deviation function which is invariant for the zero pressure gradient case. Substituting (18) in the last equation gives

$$\frac{u}{u_\tau} = \frac{1}{\kappa}\log_e\left(\frac{y}{\delta}\right) + g\left[\frac{y}{\delta}\right] - D + A.$$

At $y = \delta$, $u = U_1$ and hence $U_1/u_\tau = g[1] - D + A$. Hence the local skin friction is constant for the layer. Also, (19) can be written as $u/U_1 = \Phi[y/\delta]$ where Φ is a universal function and it then follows that the momentum thickness (θ), displacement thickness (δ^*), 99 % thickness (δ) and Clauser's (1954) thickness (Δ_c) are all proportional to each other. These facts have several corollaries. (ii) From the von Kármán momentum integral equation for a zero pressure gradient layer it follows for this particular layer that θ is proportional to the development length x and hence δ, δ^*, Δ_c are also proportional to x. (iii) The assumption that ϵ is proportional to δ now also implies that it is proportional to x, δ^*, θ, and Δ_c. (iv) Rotta (1962) noted that the exact theoretical dependence of the velocity defect law is $(U_1 - u)/u_\tau = \Phi_1[y/\delta, u_\tau/U_1]$ but that experimental results indicate that the effect of u_τ/U_1 is a weak one. He then examined the theoretical conditions to be fulfilled to obtain an exact 'self-preserving' or 'equilibrium' layer and found that both the Clauser (1954) equilibrium parameter $(\delta^*/\tau_0)/(dp/dx)$ and u_τ/U_1 must be held constant. Thus although any zero pressure gradient boundary layer will have a constant Clauser equilibrium parameter (as $dp/dx = 0$) the flow will only be approximately self-preserving unless u_τ/U_1 is also constant. Rotta suggests as an example of exact self-preserving flow, a zero pressure gradient boundary layer on a 'k' type rough wall in which the height of the roughness elements varies with x such that u_τ/U_1 is constant. No experimental results of such a layer have been reported.

The boundary layer considered here conforms theoretically to Rotta's condition for exact self-preserving flow.

4. Description of experiment

Wind tunnel

The tests were performed in a large wind tunnel of the return circuit closed working section type with a turbulence intensity in the working section of 0·3 %. The fan speed was controlled to within 0·1 % of the selected value.

A long flat plate was installed in the working section which had the same structural details as shown in Perry (1966, figure 1). The plate spanned the full height of the tunnel and was mounted such that its angle of attack could be varied through a wide range. Felt seals between the edges of the plate and the tunnel isolated the flow on each side of the plate. For strong adverse pressure gradient tests a blister was constructed on the tunnel wall opposite the trailing edge of the plate to prevent flow separation. A standard Prandtl tube placed near the leading edge of the plate gave a reference dynamic head that was maintained within $\frac{1}{2}$ % of the selected value throughout each series of runs.

Roughness

A two-dimensional roughness pattern was used. There were three sizes of roughness which had nominal heights of $\frac{1}{8}$ in., $\frac{1}{2}$ in. and 1 in. The $\frac{1}{8}$ in. roughness was machined out of a rolled aluminium plate (10 ft. long by 3 ft. wide) that was clamped to the main plate. Corner fillets were fitted to prevent corner vortices from forming. The ends of each groove were sealed to isolate the flow in each groove.

Plate construction	Nominal height of elements		k in.	b in.	W in.	L in.
Aluminium	$\frac{1}{8}$ in.	Mean	0·123	0·990	0·112	36
	(*DIII* Series)	Standard deviation	$1{\cdot}9 \times 10^{-3}$	$8{\cdot}3 \times 10^{-4}$	$8{\cdot}0 \times 10^{-4}$	—
Timber	$\frac{1}{2}$ in.	Mean	0·498	—	—	48
	(*DII* Series)	Standard deviation	$3{\cdot}6 \times 10^{-3}$	—	—	—
	1 in.	Mean	0·991	0·879	0·934	47
	(*DI* Series)	Standard deviation	$4{\cdot}7 \times 10^{-3}$	$6{\cdot}61 \times 10^{-3}$	$1{\cdot}54 \times 10^{-2}$	—

TABLE 1

The nominally $\frac{1}{2}$ in. and 1 in. scale roughness elements were made from accurately machined timber which were glued to the main plate. The $\frac{1}{2}$ in. elements were graded along the plate, the leading element being the lowest and the trailing element the highest. The 1 in. elements were not so graded. A number of random measurements of the salient features of the roughness geometry (k, b, W) were taken on both the wooden and aluminium plates. Values of the mean and standard deviations of the distribution of these quantities are given in table 1.

Maull & East (1963) reported three-dimensional flow behaviour in a large single groove under a thin boundary layer for k/W outside the range

$$0{\cdot}875 < k/W < 1{\cdot}2.$$

Kistler & Tan (1967) also found cellular flow in a similar experimental situation for $k/W < 2{\cdot}5$. In the present work k/W had a nominal value of 1·11. As it was important that two-dimensional flow patterns existed in the wall slots, extensive flow visualization tests were performed on the flow in the cavities. The tests, involving dye streaks, tufting the cavity walls, smoke and tufted probes did not reveal any cellular flow patterns across the plate.

For all scales of roughness the plate was fitted with a smooth leading edge, shown in the inset of figure 3. The crest of the first element was at the same level as the leading edge to prevent a local separation bubble.

Procedure

Twelve of the wooden roughness elements spaced along the plate were made removable so that an element fitted with pressure-tapped pads could be inserted into the roughness pattern. The pressure-tapped pads (shown in figure 5) were

made of brass tubes soldered together and drilled at varying distances up the height of the element. A pair of corresponding tubes from each side of the element was connected in turn to a Chattock manometer enabling the pressure difference profile across the element to be measured to an accuracy of $\pm 0{\cdot}0003$ inches of water. The elements of the aluminium plate were not pressure tapped.

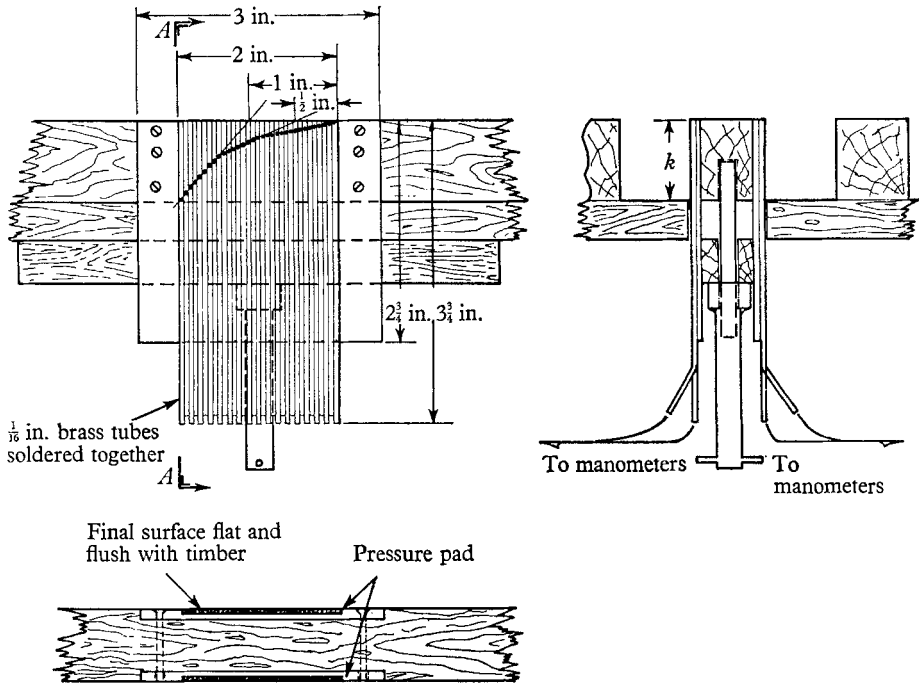

FIGURE 5. Diagram of pressure-tapped roughness element.

At these twelve stations mean velocity profiles were taken on the plate centre line using the automatic traversing and plotting system developed by one of us (Perry 1966). The system was periodically compared with a standard Prandtl tube and Betz manometer system and the errors were always less than 1 %. The repeatability of the profiles were to the same accuracy.

Three of the tests were in strong adverse pressure gradients. These pressure gradients were measured in great detail (approximately 80 readings were taken for each gradient) with a special probe on a longitudinal traverse. The probe consisted of two tubes soldered together and mounted on a long sting to remove it from the pressure field of the traverse.

Each tube was drilled with a static pressure hole and the holes in the two tubes were spaced 1·80 in. apart. This distance corresponds to $n\lambda$ where $n = 1$ for $k = 1$ in. and $n = 2$ for $k = \frac{1}{2}$ in. With the probe positioned about $0{\cdot}8\delta$ away from the wall the pressure difference between the two holes was read on a Chattock manometer. The small errors due to the distortion around the probe and sting were measured, and allowed for. The pressure at each hole of the probe was compared at the same streamwise position with a static stream tube fixed to the plate. The stream tube was repositioned along the plate for each major

repositioning of the pressure gradient probe traversing system. Nominally zero pressure gradients were checked at twelve positions along the plate with standard Prandtl tubes and a Betz manometer.

The flow over the rough surface was investigated visually using a tufted probe, dye streaks and smoke. For all plate settings the flow was found to be steady, attached and two-dimensional across the complete width of the roughened plate. Mean velocity profiles taken above and below the centre line of the plate agreed with the centre-line profile within the accuracy of the recording system.

Profiles taken at a fixed position but with tunnel speeds varying from 67 ft./sec to 106 ft./sec also agreed within the accuracy of the recording system.

5. Results

Determination of wall shear stress

The wall shear stress for the boundary layers over the 1 in. and $\frac{1}{2}$ in. timber roughness elements was evaluated by analyzing the control volume around a single element shown in figure 6. The effective average wall shear stress is

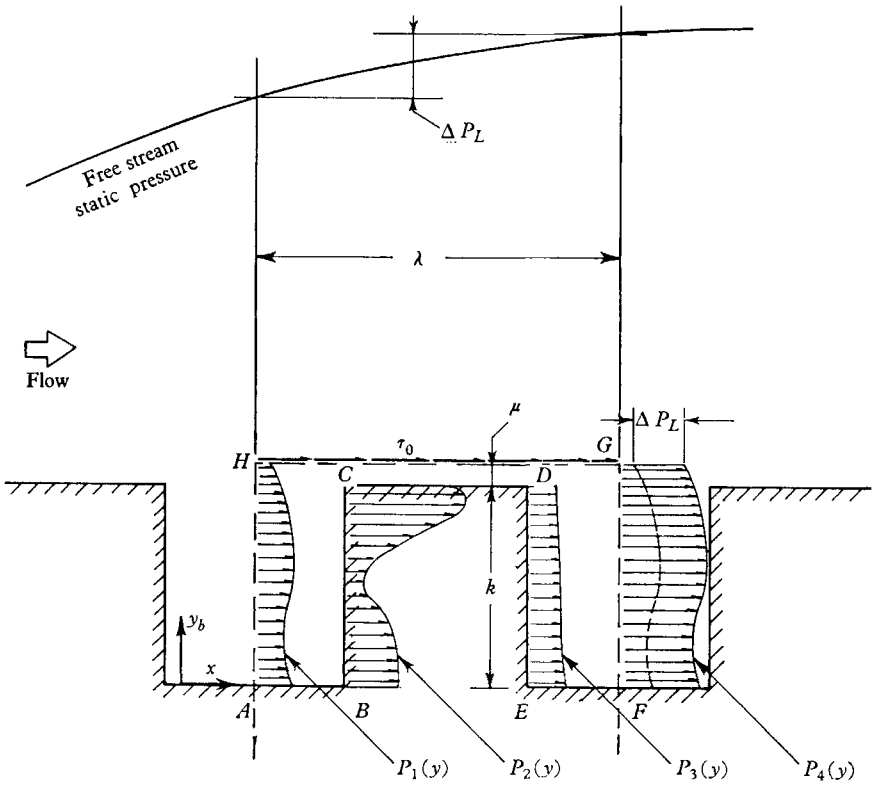

FIGURE 6. Control volume used to determine the effective wall shear stress.

assumed to act along a surface HG positioned a distance μ above the crest of the elements, where μ is small compared with k. From the work of Roshko (1955) and Fox (1964) the shear on the cavity walls $ABCDEF$ (figure 6) are assumed negligible compared with the pressure forces acting. Flow patterns in successive

showed up clearly in this test and appear flattened as shown in figure 10. The small separation bubble on the leading edge of the crest of the roughness element has been previously noted by Fox.

Determination of $\Delta u/u_\tau$ and ϵ

With a known value of skin-friction coefficient, the roughness function and the error in origin of the velocity profiles were determined using a modified Clauser plot as discussed in §2.

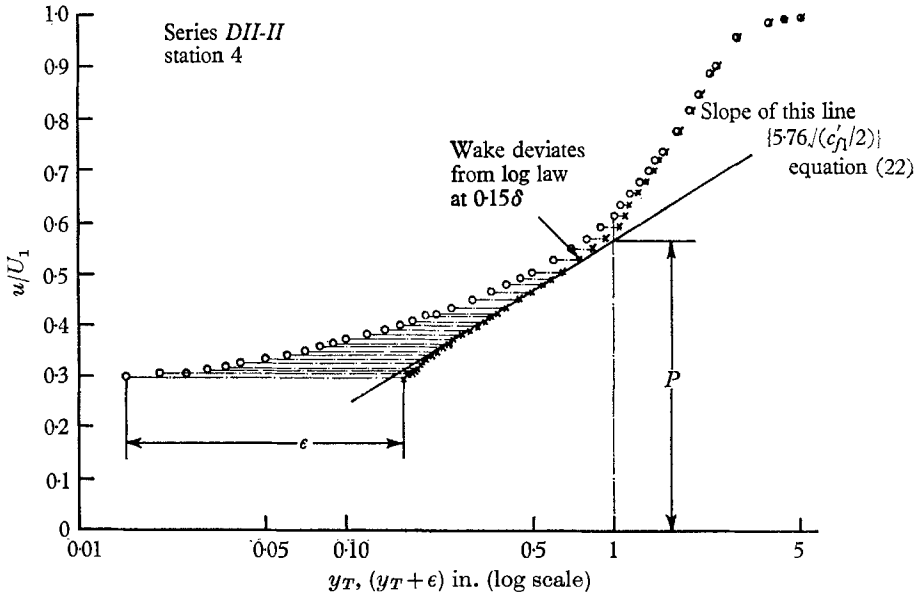

FIGURE 11. Example of velocity profile reduction technique.

Near the wall (14) is valid and for $\kappa = 0{\cdot}40$ and $A = 5{\cdot}1$† can be written

$$\frac{u}{U_1} = 5{\cdot}76\sqrt{\frac{c'_{f1}}{2}}\log_{10}\left\{\frac{(y_T+\epsilon)U_1}{\nu}\right\} + 5{\cdot}76\sqrt{\frac{c'_{f1}}{2}}\log_{10}\left(\sqrt{\frac{c'_{f1}}{2}}\right) + 5{\cdot}1\sqrt{\frac{c'_{f1}}{2}} - \frac{\Delta u}{u_\tau}\sqrt{\frac{c'_{f1}}{2}}, \tag{22}$$

where c'_{f1} is the local skin-friction coefficient. It is shown by Perry & Joubert (1963) that $\Delta u/u_\tau$ is then given by

$$\frac{\Delta u}{u_\tau} = 5{\cdot}76\log_{10}\left(\frac{U_1}{\nu}\sqrt{\frac{c'_{f1}}{2}}\right) - P\sqrt{\frac{c'_{f1}}{2}} - 1{\cdot}11, \tag{23}$$

where P is the value of u/U_1 given by (22) for $y_T = 1$ in. To find ϵ and $\Delta u/u_\tau$ the raw velocity profiles were first plotted on axes u/U_1 *versus* $\log_{10} y_T$ as shown in figure 11. The required slope of the final logarithmic distribution ($5{\cdot}76\sqrt{\frac{1}{2}c'_{f1}}$ by (22)) was then calculated using the value for the local skin-friction coefficient that had been previously determined by the pressure-tapped roughness element

† Perry & Joubert used $\kappa = 0{\cdot}41$, $A = 4{\cdot}9$ giving slightly different constants in equations (22) and (23).

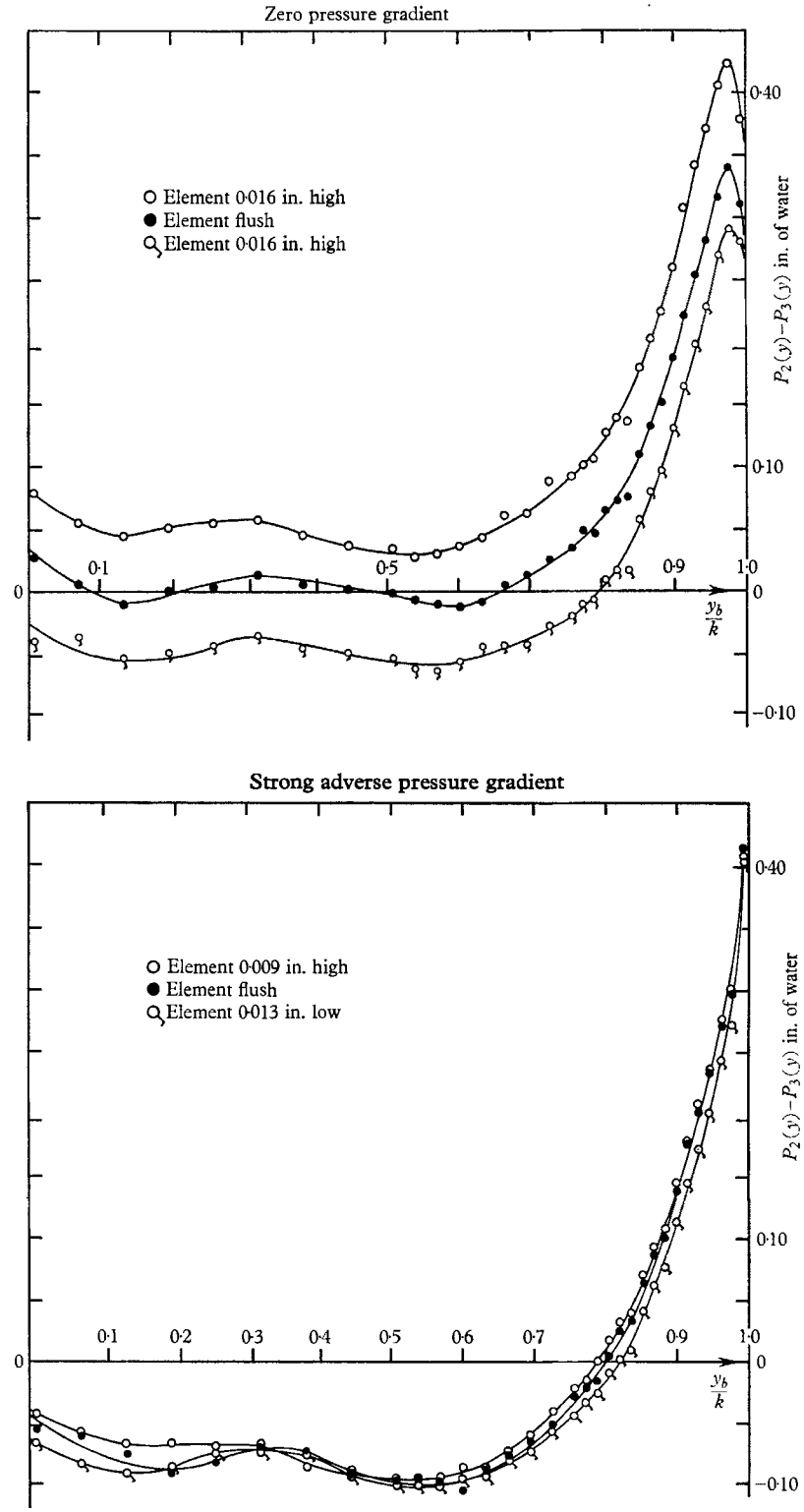

FIGURE 7. Effect of vertical misalignment of the crest of the pressure-tapped roughness element on the pressure difference profile. '*d*' type roughness.

the roughness elements (k) but some profiles were taken near the leading edge of the plate where the boundary layers were relatively thin.

Pressure difference profiles are shown in figure 7 where $(P_2(y)-P_3(y))$ is plotted against y_b/k. Profiles of $(P_2(y)-P_3(y))/\tau_0$ *versus* y_b/k are not universal as the pressure gradient has an effect that cannot be accounted for by a simple subtraction. Unlike the analysis leading to (20), the problem here is to account for pressure gradient effects over a distance less than λ.

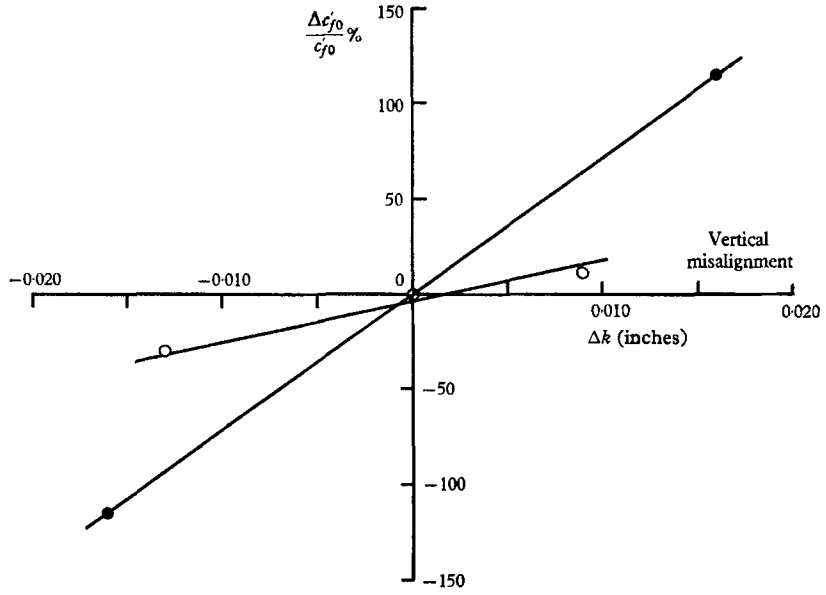

FIGURE 8. Percentage error in skin-friction coefficient due to vertical misalignment of pressure-tapped roughness element. ○, strong adverse pressure gradient; ●, zero pressure gradient.

The variation of the measured C_{D0} due to misalignment of the pressure-tapped element in the array was tested. The value of C_{D0} was found to be only moderately sensitive to longitudinal errors in position; a 1 % error in the x-direction resulted in a 1 % change in drag coefficient. However, vertical alignment of the crest of the pressure-tapped element with respect to the crests of the neighbouring elements was critical. The effect of a misalignment was to shift the curves bodily up and down as shown in figure 7. This shift depends on the degree of vertical misalignment and the nature of the pressure gradient. In figure 8 the percentage change in c'_{f0} is plotted against vertical misalignment of the crest of the pressure-tapped element in a zero and strong adverse pressure gradient. As only the 1 in. elements were used for the test it is not known whether the error in drag depends on the absolute value of the vertical misalignment or on the ratio of the misalignment to the size of the roughness. Kistler & Tan reported a similar result for a single cavity. In a zero pressure gradient boundary layer they found that a 1 % rounding of the downstream edge of the cavity (the stagnation corner) caused a 10 % change in cavity drag. As the crest alignment was held locally to $\pm$ 0·003 in. during measurements, possible errors in drag coefficient were small for the adverse

pressure gradient cases. The same tolerance on vertical alignment of the crests in a zero pressure gradient layer made the method unreliable with timber elements. A machined aluminium plate was therefore used to ensure that the element crests were aligned more accurately. However, since this plate could not be pressure tapped the momentum integral method was used to determine skin friction.

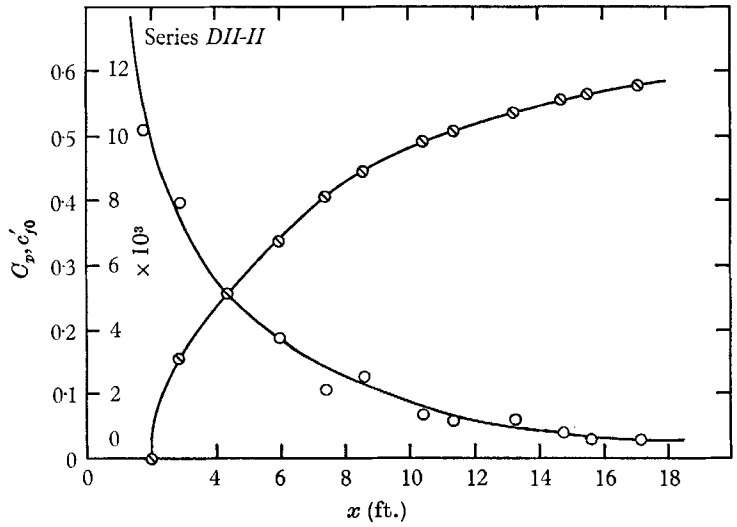

FIGURE 9. Typical skin-friction coefficient and free stream pressure coefficient distribution along the plate (strong adverse pressure gradient). ○, c'_{f0}; ⊘, C_p.

The values thus determined for skin-friction coefficient were plotted against distance from the leading edge of the plate and a faired in curve was drawn. These faired in values were used in subsequent data reduction. A typical set of results for a test series is shown in figure 9. Figure 9 also shows the longitudinal free stream pressure variation for the same series of tests.

Flow visualization

The flow on the surface of the roughness geometry was qualitatively investigated using a weak suspension of titanium dioxide in kerosene. The suspension was painted onto a small area of the plate covering two or three consecutive wavelengths of the roughness geometry. The wind tunnel was turned on immediately causing the suspension to move in the direction of the local airflow while the kerosene was being evaporated. When all the kerosene was evaporated streaks of titanium dioxide were left on the surfaces. As the plate was mounted vertically in the tunnel the suspension had an additional uniform velocity towards the floor of the tunnel. The orientation and angle of the final streaks thus gave an indication of local surface flow direction and its relative speed. Sketches of a typical set of streak patterns are shown in figure 10 with the deduced flow pattern around the roughness geometry shown below them. Although the test was repeated at five positions over the full length of the plate, no substantial changes in the patterns were noted. The tests were performed at one adverse pressure gradient setting of the plate only.

The areas on the sketches that are shaded represent positions of heavy titanian dioxide deposit where individual streaklines could not be discerned. Similarly, blank areas indicate positions of little to no titanium dioxide deposit. From the angles of the streaklines inferences can be made about the relative surface velocities around the cavities. The highest velocity is over the crest of the elements except for a small region near its leading edge where the flow appears to be separated. The main eddy within the cavity has a velocity of the order of

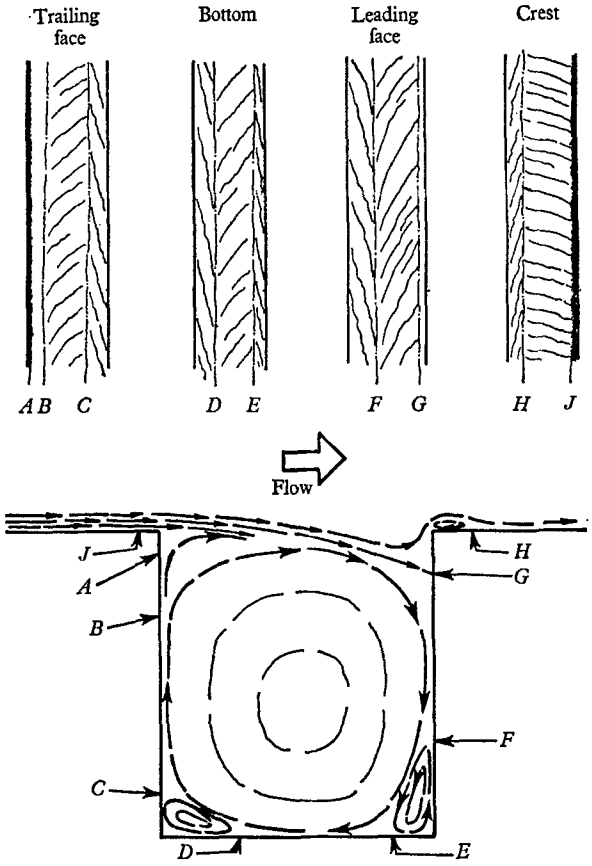

FIGURE 10. Surface flow patterns around '*d*' type roughness geometry.

half that of the crest velocity. The velocities of the small eddies in the corners of the cavity appear to be an order less than that of the main eddy. The final sketch of the cavity flow differs only slightly from the descriptions given by Roshko (1955), Fox (1964) or Haughen & Dhanak (1966) for single cavities and the description given by Liu, Kline & Johnston (1966) for rough channel flow. However, in the case considered here the stagnation streamline appears to penetrate the cavity further than in the papers cited above. This may be due to the external pressure gradient that was absent in the previous studies. The small 'roller' vortices in the corners of the cavity, that were conjectured by previous workers,

showed up clearly in this test and appear flattened as shown in figure 10. The small separation bubble on the leading edge of the crest of the roughness element has been previously noted by Fox.

Determination of $\Delta u/u_\tau$ and ϵ

With a known value of skin-friction coefficient, the roughness function and the error in origin of the velocity profiles were determined using a modified Clauser plot as discussed in §2.

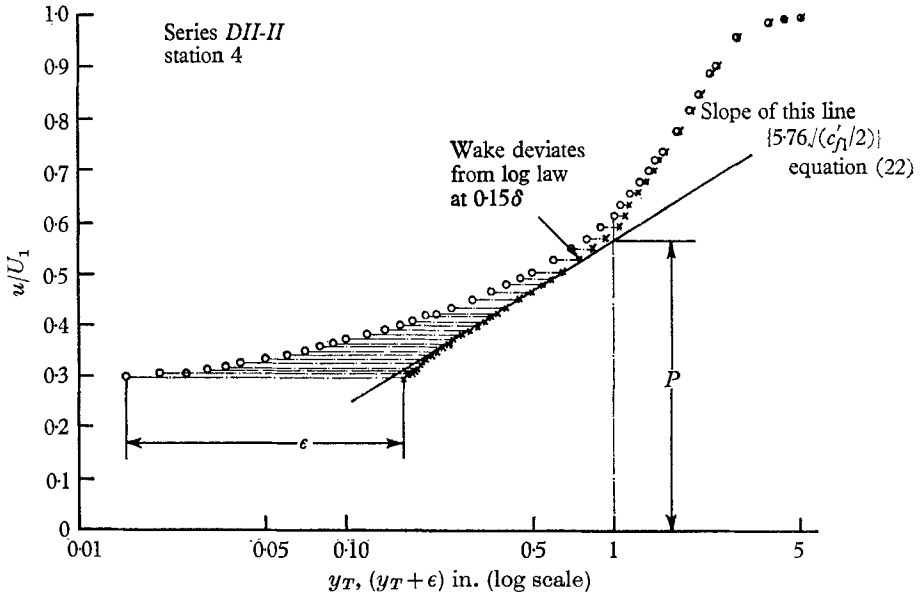

FIGURE 11. Example of velocity profile reduction technique.

Near the wall (14) is valid and for $\kappa = 0{\cdot}40$ and $A = 5{\cdot}1$† can be written

$$\frac{u}{U_1} = 5{\cdot}76\sqrt{\frac{c'_{f1}}{2}}\log_{10}\left\{\frac{(y_T+\epsilon)U_1}{\nu}\right\} + 5{\cdot}76\sqrt{\frac{c'_{f1}}{2}}\log_{10}\left(\sqrt{\frac{c'_{f1}}{2}}\right) + 5{\cdot}1\sqrt{\frac{c'_{f1}}{2}} - \frac{\Delta u}{u_\tau}\sqrt{\frac{c'_{f1}}{2}}, \tag{22}$$

where c'_{f1} is the local skin-friction coefficient. It is shown by Perry & Joubert (1963) that $\Delta u/u_\tau$ is then given by

$$\frac{\Delta u}{u_\tau} = 5{\cdot}76\log_{10}\left(\frac{U_1}{\nu}\sqrt{\frac{c'_{f1}}{2}}\right) - P\sqrt{\frac{c'_{f1}}{2}} - 1{\cdot}11, \tag{23}$$

where P is the value of u/U_1 given by (22) for $y_T = 1$ in. To find ϵ and $\Delta u/u_\tau$ the raw velocity profiles were first plotted on axes u/U_1 *versus* $\log_{10} y_T$ as shown in figure 11. The required slope of the final logarithmic distribution ($5{\cdot}76\sqrt{\frac{1}{2}c'_{f1}}$ by (22)) was then calculated using the value for the local skin-friction coefficient that had been previously determined by the pressure-tapped roughness element

† Perry & Joubert used $\kappa = 0{\cdot}41$, $A = 4{\cdot}9$ giving slightly different constants in equations (22) and (23).

or momentum integral method. Values of ϵ were then added to the abscissae of the raw profile in a trial-and-error process until a value of ϵ was obtained that gave a straight line of the required slope. In general the final profile approximated closely to a straight line up to 0·10 to 0·15 of the boundary-layer thickness where the wake deviated from the logarithmic distribution. A complete set of final profiles are shown in figure 12. These final profiles show a slight deviation from the logarithmic distribution line for a thin layer near the origin of the profile. This is a consequence of the velocity probe being set up on the leading edge of a roughness element crest at the start of every velocity profile traverse. As the flow visualization tests indicated a small separation bubble in this region these first few points probably correspond to this separated flow.

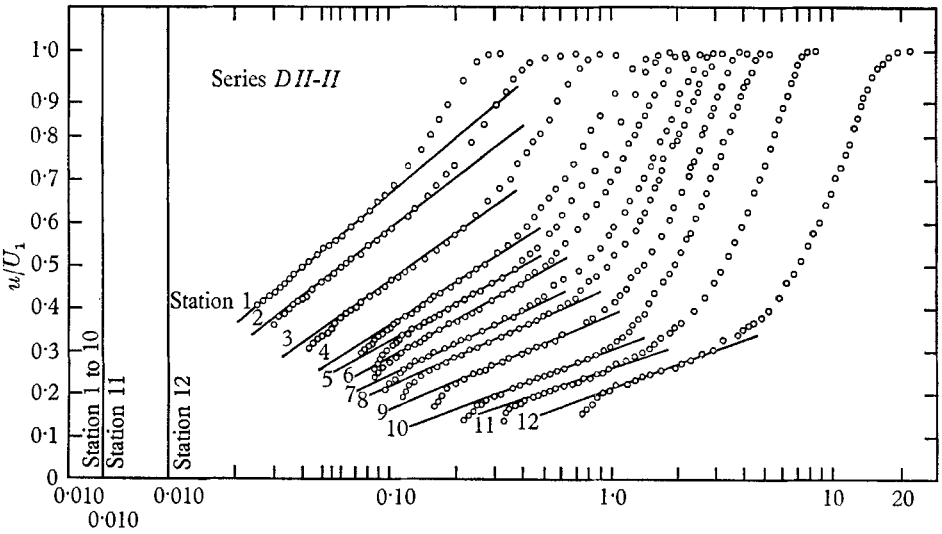

FIGURE 12. Typical set of final velocity profiles on a '*d*' type rough wall in an adverse pressure gradient. Experimental points are left out for clarity in profiles of stations 6 to 12.

With the position of the velocity profile fixed on the graph, the intercept of the straight line representing the logarithmic distribution and the $y_T = 1$ in. ordinate gave P and hence $\Delta u/u_\tau$ by (23). Experimental scatter within the velocity profile meant that there was usually a small range of positions on the graph for the final profile. In addition the tolerance in setting up the origin of the velocity profile probe was significant and this widened the range of ϵ particularly for cases with small ϵ.

Adverse pressure gradient results

The skin-friction coefficient was determined by the drag-measurement technique for all three adverse pressure gradient runs. The values obtained decreased monotonically down the plate as illustrated in figure 9.

The error in origin (ϵ) varied with x in each case. Two sets of results for strong adverse pressure gradients (Series *DII–II* and *DI–I*) are shown in figure 13.

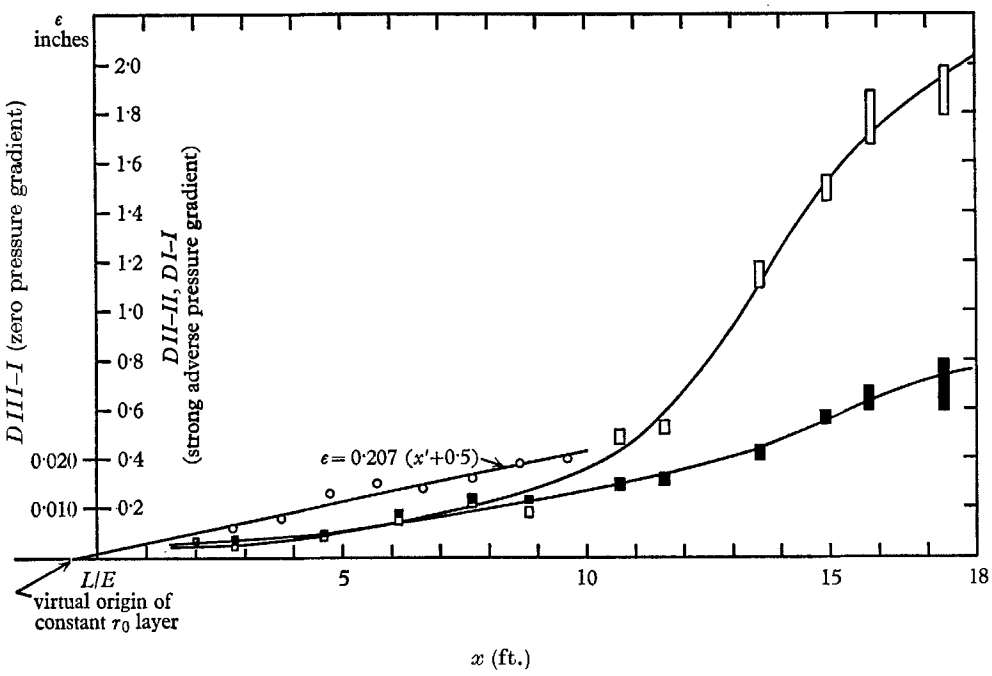

FIGURE 13. Examples of the variation of ϵ along the plate for zero and strong adverse pressure gradients. ○, *D III–I*; □, *D I–I*; ■, *D II–II*.

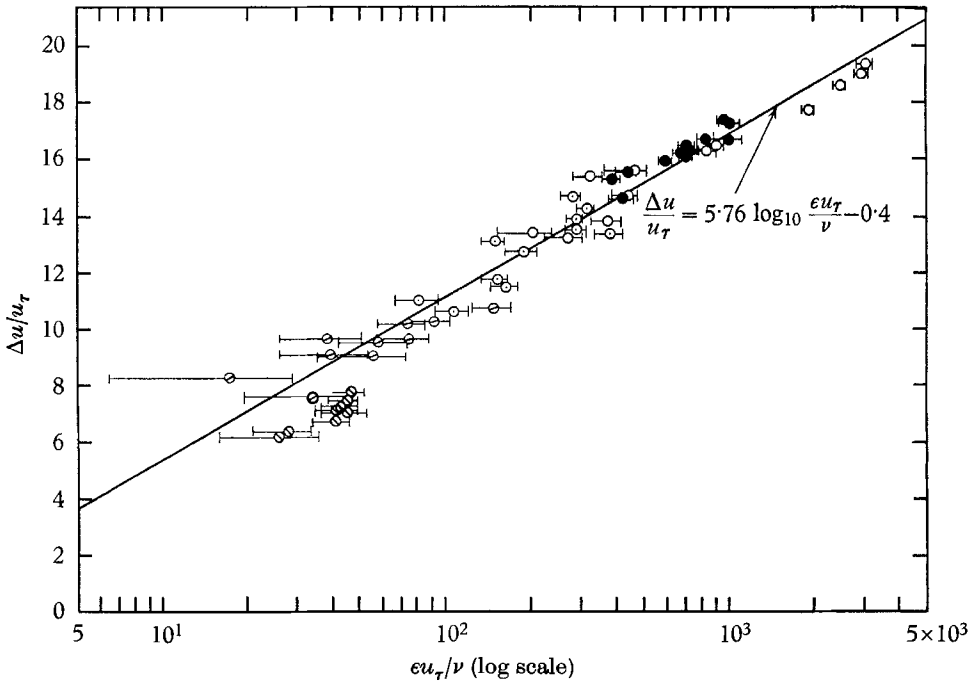

FIGURE 14. Roughness function 'd' type roughness. |—○—|, *D I–I* (strong adverse pressure gradient); |—⊙—|, *D I–II* (moderately strong adverse pressure gradient); |—⊘—|, *D I–III* (zero pressure gradient); |—●—|, *D II–II* (strong adverse pressure gradient); |—⊗—|, *D III–I* zero pressure gradient. Values of k for each series are given in table 1.

The values of ϵ near the trailing edge of the plate are in these cases greater than the height of the elements. This means that the flow in this region 'feels' an origin below the base of the roughness elements.

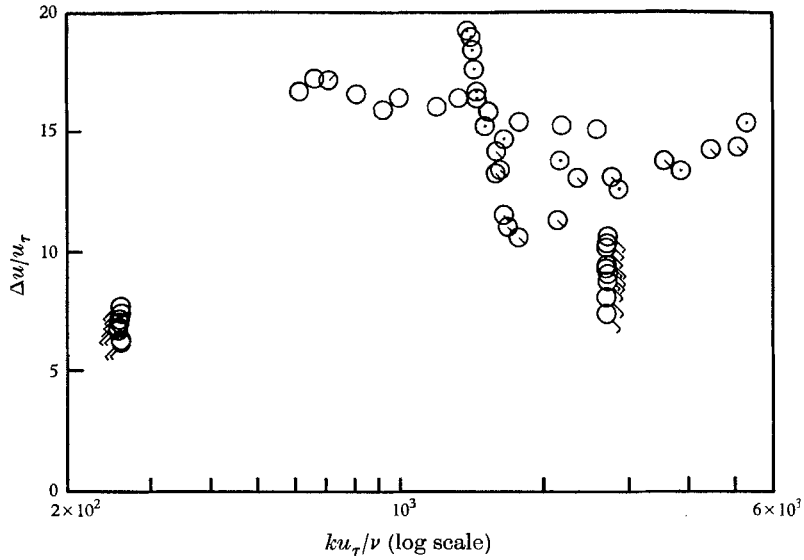

FIGURE 15. Roughness function for 'd' type roughness plotted using Clauser's (1954) parameters. ⊙, *D I–I*; ○, *D I–II*; ○, *D I–III*; ○, *D II–II*; ○, *D III–I*.

Figure 14 shows the roughness function $\Delta u/u_\tau$ plotted against $\log_{10}\epsilon u_\tau/\nu$. The results agree closely with

$$\frac{\Delta u}{u_\tau} = 5{\cdot}76\log_{10}\left(\frac{\epsilon u_\tau}{\nu}\right) - 0{\cdot}4, \tag{24}$$

which is the form given by the analysis in §3 (equation (17)). As the range of uncertainty in the values of ϵ appears more pronounced on the logarithmic scale for small values of ϵ, the position of the theoretical line is verified more convincingly at the large values of $\epsilon u_\tau/\nu$. If these 'd' type results are plotted on axes $\Delta u/u_\tau$ *versus* ku_τ/ν (which were first used by Clauser (1954)) they give very large scatter with no apparent correlation as shown in figure 15.

Zero pressure gradient results

The skin friction coefficients for the test at zero pressure gradient using the aluminium plate ($k = \frac{1}{8}$ in. nom.) were determined using the momentum integral equation. Figure 16 shows the momentum thickness of this boundary layer plotted against distance from the leading edge of the plate (x). The actual position used for the leading edge is shown in figure 3. After a short distance down the rough plate the experimental points give a good fit to a straight line. This implies a constant wall shear stress.

The determination of ϵ, by the method previously described, gave ranges for its value that were proportionately larger than those obtained for the adverse pressure gradient cases. This was a consequence of the Clauser plot which was

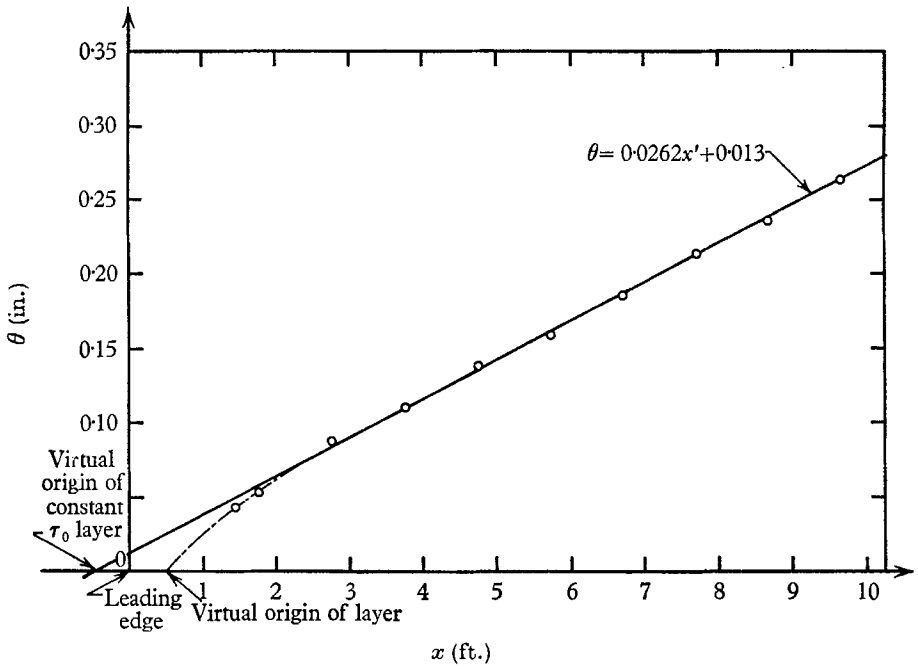

FIGURE 16. Momentum thickness, variation along the plate for a zero pressure gradient boundary layer on a '*d*' type rough wall.

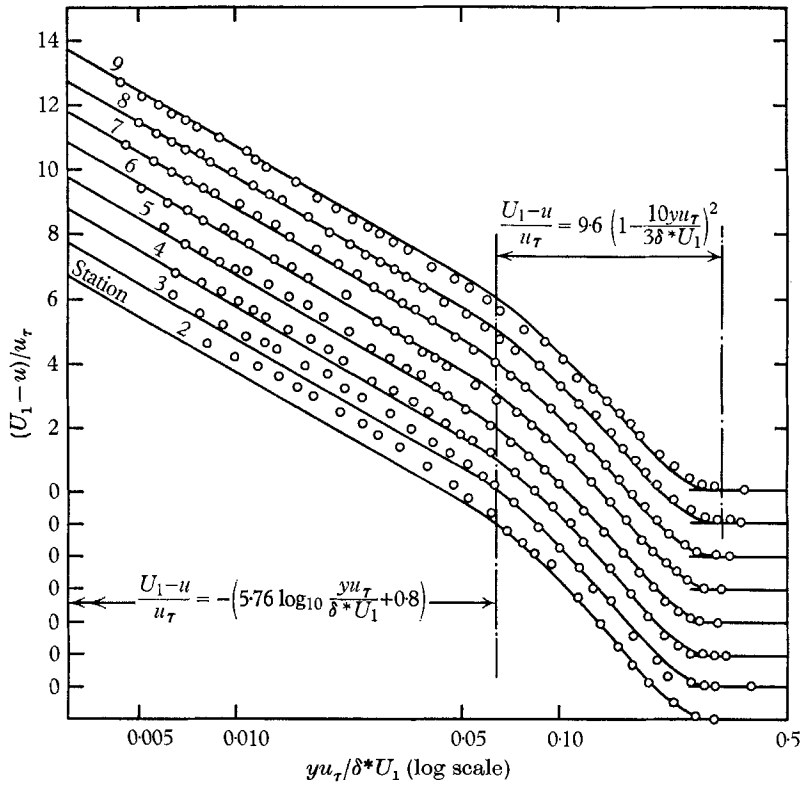

FIGURE 17. Velocity profiles compared with Hama's (1954) form of the velocity defect law. '*d*' type roughness in a zero pressure gradient.

found to be proportionately more accurate for large ϵ than small ϵ. The velocity profiles were then compared with Hama's (1954) equation for the velocity defect law (figure 17). For every profile the value of ϵ to be added to y was chosen from within the range of values determined by the Clauser plot method that gave the best fit to Hama's equation. These values of ϵ were used for all subsequent

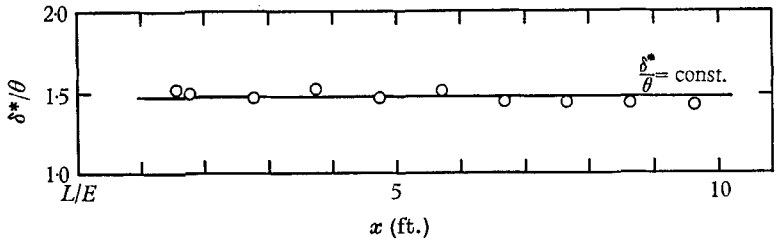

FIGURE 18. Form factor variation along the plate. '*d*' type roughness in a zero pressure gradient.

results and are shown plotted against x in figure 13 (series *DIII–I*). A consequence of the work in § 3 in this type of boundary layer is that if ϵ is proportional to the boundary-layer thickness then it should also be proportional to x with the same virtual origin as the constant wall shear stress layer. This virtual origin was determined from the straight line equation fitted to the values of the boundary-layer momentum thickness. With this origin a straight line was fitted to the values of ϵ which is also shown on figure 13. Considering the small values of ϵ the scatter of points around the line seems reasonable. Other consequences of the work in § 3 are, firstly, that the boundary-layer thicknesses δ, δ^*, θ, Δ_c are proportional to each other. Figure 18 shows that the form factor δ^*/θ is approximately constant with distance down the plate. Secondly, the velocity profiles may be simply described by $u/U_1 = \psi[y/l]$, where l can be either δ, δ^*, θ or Δ_c and ψ is a universal function. The profiles are plotted on axes u/U_1 *versus* y/θ and compared with the Hama formulation of the velocity defect law expressed in terms of these variables in figure 19.

The roughness function results correlate with both (20) (shown in figure 14) and an equation of the form given by (18). Figure 20 shows these results plotted on axes $\Delta u_\tau/\nu$ *versus* $\Delta_c u_\tau/\nu$ where Δ was used instead of δ as it is more accurate since it is defined on integral basis.

The results show a reasonably good fit with a straight line of slope 1 : 5·76 (which is the theoretically predicted value) but there is an insufficient range of results to be conclusive. The equation to the line shown on the graph is

$$\Delta u/u_\tau = 5{\cdot}76 \log_{10}(\Delta_c u_\tau/\nu) - 16{\cdot}9.$$

For comparison the results are also shown plotted against the Clauser parameter ku_τ/ν and in this case no correlation is apparent.

The tests using timber elements in zero pressure gradient were largely unsuccessful as even with the crests locally aligned to within 0·003 in. the value of skin friction coefficient showed large scatter. The boundary layer was found to thicken more rapidly than the same layer on the aluminium plate as the elements were aligned accurately only in the neighbourhood of the measuring stations. The

momentum thickness of this boundary layer therefore did not correspond with the measured skin friction coefficient because the outer flow had a history unrelated to the measured local skin-friction coefficient. In spite of these facts the measured skin friction coefficient for the pressure tapped timber elements had an average value of $4{\cdot}11 \times 10^{-3}$ which compared favourably with the constant value of $4{\cdot}36 \times 10^{-3}$ obtained from tests on the aluminium plate. Accordingly the inner (logarithmic) portions of the velocity profiles were reduced using a constant skin friction coefficient of $4{\cdot}36 \times 10^{-3}$. The results are plotted on figure 14 for completeness. These results must be regarded as uncertain.

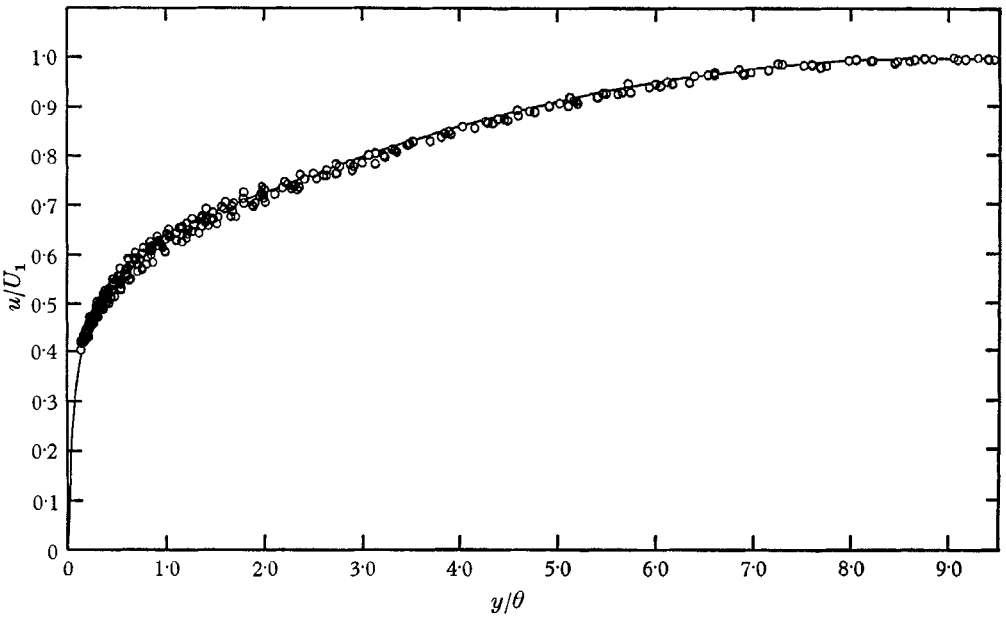

FIGURE 19. Velocity profiles plotted in the form $u/U_1 = \psi(y/\theta)$. 'd' type roughness in a zero pressure gradient.

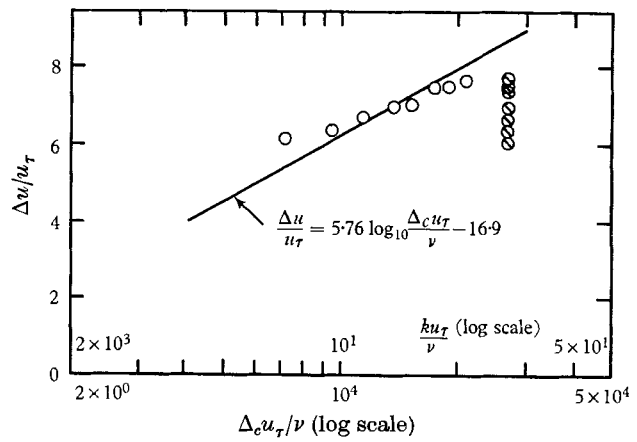

FIGURE 20. Roughness function results for 'd' type roughness in a zero pressure gradient plotted against both $\Delta u_\tau/\nu$ and the Clauser (1954) parameter ku_τ/ν. ○, $\Delta u/u_\tau$ *versus* $\Delta_c u_\tau/\nu$; ⊙, $\Delta u/u_\tau$ *versus* ku_τ/ν.

6. Checking the method

The adverse pressure gradient results in this paper depend on the validity of the assumptions and method used to evaluate 'the effective wall shear stress'. There are several points on which this simple analysis could be criticized. First, the streamlines close to the crests of the elements are most probably wavy as mentioned in § 5. Also it is plausible that the shear stress, determined by the drag measurement technique, should be evaluated at the local effective origin of the layer. This can be done by assuming a linear stress distribution $\tau/\rho = \tau_0/\rho + \chi y_T$ (where χ is approximately equal to the kinematic pressure gradient $1/\rho\, dp/dx$) and extrapolating to $y_T = -\epsilon$. Shear stresses were calculated in this way but the values were extremely small and often negative. The shear stress evaluated at the crests of the elements that has been used in this paper relies heavily on experimental justification. Therefore, although the results presented so far appear consistent within themselves, further independent experimental checks were considered necessary.

Every second element was removed from the plate fitted with the 1 in. timber elements giving a geometry with a nominal pitch to height ratio of 3·6 to 1. This represents a geometry only 10 % different in λ/k to that used by Moore (1951), Hama (1954) and Perry & Joubert (1963) and is thus a well-documented case of 'k' type roughness. To obtain a large variation of the parameters $\Delta u/u_\tau$ and ku_τ/ν the plate was set in a severe adverse pressure gradient.

First, surface flow visualization tests were carried out as before and sketches of the resulting patterns are shown in figure 21. Again no significant changes in the patterns were discerned over the complete length of the plate. The flow around the roughness geometry implied from these patterns is also shown in figure 21 and it is firstly noted that there is no evidence of a stagnation streamline on the leading face of the cavity. The flow in this region seems to divide about a streamline near the front of the crest of the element although this was not shown conclusively by the streaklines. The flow around this roughness geometry is markedly different to the 'd' type case in that the flow structure is not confined to the cavity. Other differences are, firstly, the absence of a separation bubble on the leading edge of the crest and secondly the existence of a pocket of nearly stagnant fluid near the trailing face of the cavity. The relative surface velocities appear to be of approximately the same orders as in the 'd' type case.

The roughness function was then evaluated for this case of 'k' type roughness in a strong adverse pressure gradient using the methods discussed previously. The first four stations on the plate did not yield a solution by the Clauser plot technique as there were insufficient experimental points or none at all falling on the logarithmic straight line. This was due to the fact that the error in origin was large compared with the boundary-layer thickness, implying that the majority of the logarithmic velocity distribution would have existed below the crests of the elements. Even if a solution was possible using another technique the results would be suspect as the simple Nikuradse model of the roughness effect being confined to a *thin* wall layer would not be valid. The error in origin (ϵ) was found to have an average value of $0{\cdot}75k$ which agrees closely with the data of Perry &

Joubert (1963) and Moore (1951) (who gave approximately $0{\cdot}7k$). Some change in the proportion of k representing ϵ was to be expected as the roughness geometry was not identical to the previous studies; however, the spread in the values of

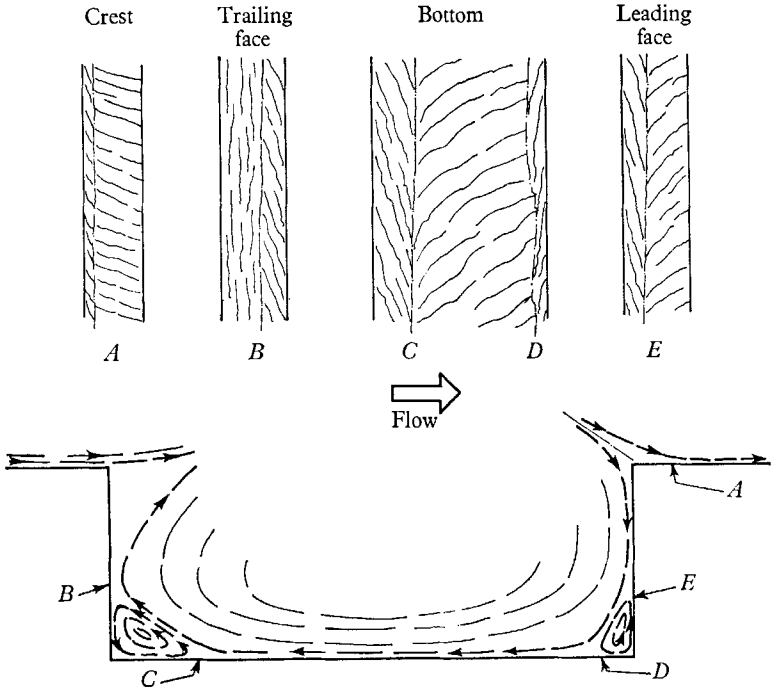

FIGURE 21. Surface flow patterns around 'k' type roughness geometry.

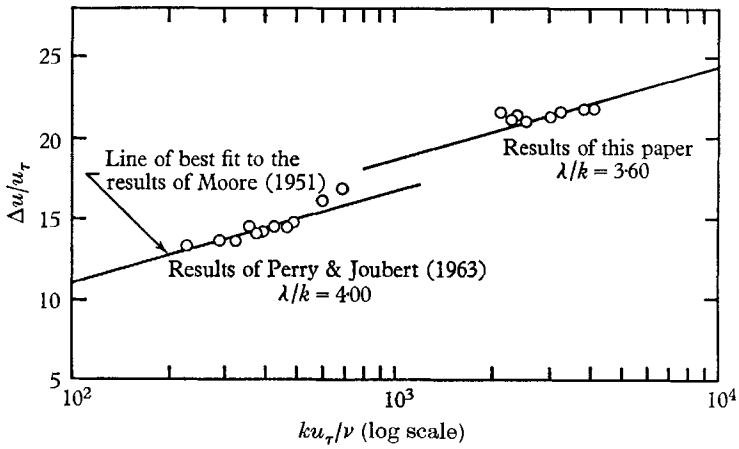

FIGURE 22. Roughness function. 'k' type roughness.

was larger than expected. Figure 22 shows the roughness function plotted against $\log_{10}(ku_\tau/\nu)$. For comparison the results of Perry & Joubert are shown as well as the line of best fit to the data of Moore. The present results show fair agreement with a line of the correct slope (1 : 5·76); however, the intercept at $\log_{10}(ku_\tau/\nu) = 0$

has a value of approximately + 1·2, whereas Perry & Joubert found a value of − 0·2. Variation in this constant can also be ascribed to the change in roughness geometry, but it is difficult to estimate what the order and even the direction of the variation should be. Work has been done using two-dimensional roughness elements at different spacings by Schlichting (1936), Betterman (1966) and Liu *et al.* (1966). However, the changes in spacing used in all these studies have been very large and results showed contradictory trends. Interpolation of these results

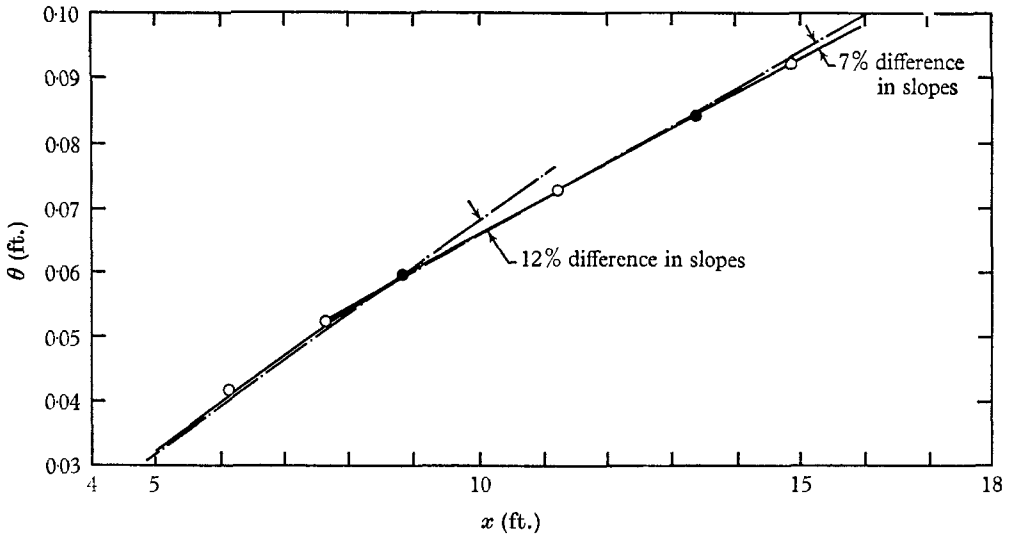

FIGURE 23. Momentum thickness variation along the plate. 'k' type roughness in a zero pressure gradient boundary layer. ○, experimental values of θ; ●, experimental values of θ and positions of drag measurement; · —· —· —, local slope of θ *versus* x by drag measurement; ——, faired-in curve of θ *versus* x.

was considered very unreliable. It was unfortunate that the 'k' type roughness geometry used by previous workers could not be used here. However, as explained earlier it was necessary to choose a 'd' type roughness geometry which would avoid three-dimensional cellular flow in the cavities as reported by Maull & East (1963) and Kistler & Tan (1967). Therefore this means of checking the method of determining skin friction and roughness function while encouraging was not conclusive.

In a zero pressure gradient it was found that, for this roughness geometry, changes in the measured drag on an element due to vertical height misalignment were undetectable for a misalignment of 0·020 in. This was probably due to the 'k' type flow patterns being basically different to the 'd' type case as observed in the surface flow visualization tests.

As a second check the wall shear determined by drag measurement, at two stations, was compared with the momentum balance of the mean velocity profiles in a zero pressure gradient. The results are shown in figure 23. As the momentum balance method involves graphical differentiation of a faired-in graph an accuracy

of the order of 10 % could be expected. The agreement obtained between the two methods was 7 and 12 % for the two stations and hence the two methods were considered to show satisfactory agreement.

Value of viscosity adopted

The value used for the viscosity of the fluid is arbitrary as variation in the viscosity simply shifts the points parallel to the mean line in figures 14, 20 and 22. The value adopted in this paper was $1{\cdot}56 \times 10^{-4}$ ft.^{2}/sec.†

7. Conclusions

(i) It appears that two major types of roughness can be distinguished, referred to here as 'k' and 'd' type. 'k' type roughness follows the Nikuradse–Clauser correlation scheme. 'd' type roughness typified by depressions or narrow lateral grooves in the wall, does not follow this correlation scheme. (ii) For fully rough flow the roughness function for both 'k' and 'd' type roughness is a function of the length of scale ϵ. The relationship can be expressed

$$\frac{\Delta u}{u_\tau} = \frac{1}{\kappa}\log_e\left(\frac{\epsilon u_\tau}{\nu}\right) + C,$$

where ϵ is that distance below the crests of the elements that the effective wall of the boundary layer must be situated in order to give the usual logarithmic distribution of velocity and C is a constant that is characteristic of the roughness.

For flow over a 'k' type rough wall ϵ is proportional to the scale (k) of the roughness.

For flow over a 'd' type rough wall ϵ is not proportional to k. However, the validity of the above equation implies that in this type of flow there is a constant surface-drag coefficient which is independent of the flow situation as in the cases of k type rough wall and smooth wall flow. (iii) For the general case of 'd' type rough-wall flow no way of predicting ϵ is known. However, for the case of pipe flow ϵ appears to be proportional to the pipe diameter and results reported here show that for zero pressure gradient boundary layers, ϵ is probably proportional to the boundary-layer thickness. One possible explanation for this is that the large-scale inactive components of the turbulence structure play a major role in determining the flow at the boundary. (iv) A zero pressure gradient boundary layer developing on a 'd' type rough wall has a constant wall shear stress and conforms to Rotta's condition of precise self-preserving flow. However, the tests reported here have a limited range and therefore cannot be conclusive. (v) Skin-friction coefficients determined by the pressure-tapped roughness element technique gave results that were self consistent and agreed with the momentum integral method for 'k' type roughness in zero pressure gradient.

The authors are indebted to the Australian Institute of Nuclear Science and Engineering and to the United States Navy for financial support of this project.

† Tabulated results of ϵ, P, $\Delta u/u_\tau$, $\epsilon u_\tau/\nu$ or ku_τ/ν, C_p, c'_{f0}, C_{D0}, and detailed results may be obtained from the authors.

REFERENCES

AMBROSE, H. H. 1954 *Proc. A.S.C.E.*, vol. 80 SEP no. 491. Discussion of *Proc. A.S.C.E.* vol. 80 SEP no. 390.

AMBROSE, H. H. 1956 *University of Tennessee, Department of Civil Engineering.* Contract N/r 811(03) Office of Naval Research, Department of the Navy.

BETTERMAN, D. 1966 *Int. J. of Heat & Mass Transf.* **9**, 153.

CLAUSER, F. H. 1954 *J. Aero. Sci.* **21**, 91.

CLAUSER, F. H. 1956 *Advances in Applied Mechanics*, vol. IV. New York: Academic Press.

COLEBROOK, C. F. & WHITE, C. M. 1937 *Proc. Roy. Soc.* A **161**, 367.

CORRISON, S. & KISTLER, A. L. 1954 *NACA* TN 3133.

COLES, D. 1956 *J. Fluid Mech.* **1**, 191.

FOX, J. 1964 *NASA* TN D-2501.

HAMA, F. R. 1954 *Trans. Soc. Nav. Arch. Mar. Engrs.* **62**, 333.

HAUGHEN, R. L. & DHANAK, A. M. 1966 *Trans. A.S.M.E. J. Appl. Mech.* 641.

HINZE, J. O. 1959 *Turbulence.* New York: McGraw-Hill.

KISTLER, A. L. & TAN, F. C. 1967 *Phys. Fluids*, **10**, no. 9. (II) S 165.

KLEBANOFF, P. S. 1955 *NACA* Rep. 1247.

LIU, C. K., KLINE, S. J. & JOHNSTON, J. P. 1966 *Stanford Univ. Dept. Mech. Engng Rep.* MD-15.

MAULL, D. J. & EAST, L. F. 1963 *J. Fluid Mech.* **16**, 620.

MILLIKAN, C. D. 1938 *Proc. 5th Int. Cong. Appl. Mech.* p. 386.

MOORE, W. L. 1951 Ph.D. Thesis. State University of Iowa.

NIKURADSE, J. 1933 *V.D.I. Forshungsheft*, no. 361, Trans. *NACA* TM 1292 (1950).

PERRY, A. E. 1964 *A.S.M.E.* Paper 64-WA/FE-31.

PERRY, A. E. 1966 *J. Fluid Mech.* **26**, 481.

PERRY, A. E. & JOUBERT, P. N. 1963 *J. Fluid Mech.* **17**, 193.

ROSHKO, A. 1955 *NACA* TN 3488.

ROTTA, J. C. 1962 *Prog. Aero Sci.*, vol. 2. Ferri-Pergamon.

SAMS, K. W. 1952 *NACA* RME 52017.

SCHLICHTING, H. 1936 *Ing. Arch.* **7**, 1. Trans. *Proc. A.S.M.E.* (1936).

STREETER, V. L. & CHU, H. 1949 *Final Rep. Project* 4918 *Armour Res. Foundation, Illinois.*

TOWNSEND, A. A. 1956 *The Structure of Turbulent Shear Flow.* Cambridge University Press.

TOWNSEND, A. A. 1961 *J. Fluid Mech.* **11**, 97.